JMEPEG (2023) 32:4796–4806
https://doi.org/10.1007/s11665-022-07481-1

1059-9495/$19.00

TECHNICAL ARTICLE

Structure and Hot Corrosion Behavior of an Al-Co-Y Co-deposited Coating on TiAl Alloy

Zekun Wei, Xuan Li, Wei Lv, Bai Ming, Yongquan Li, Xing Liu, Sheng Lai, and Fuhua Liu

Submitted: 25 June 2022 / Revised: 3 August 2022 / Accepted: 20 August 2022 / Published online: 7 October 2022

The hot corrosion behavior of Al-Co-Y co-deposited coatings on TiAl alloy was investigated in 25% NaCl + 75% K_2SO_4 molten salt at 850 °C. Results show that O, S and other corrosive media are preferentially corroded by the α_2 phase of the TiAl matrix, generating corrosion products with poor density and adhesion, resulting in rapid corrosion. The Al-Co-Y co-deposited coating specimens form a dense Al_2O_3 film during the hot corrosion incubation, which effectively improves the anti-hot corrosion performance of TiAl alloy. During hot corrosion, the Al_2O_3 film is dissolved and ruptured under the action of mixed salts, losing its protective properties.

Keywords co-deposited coating, hot corrosion, preferential corrosion, TiAl alloy

1. Introduction

γ-TiAl alloys are widely used in the aerospace, automotive and gas turbine industries because of their low density, high melting point and high-temperature mechanical properties (Ref 1, 2). However, poor heat and corrosion resistance of TiAl alloys in marine environment with high salt content in the air can lead to the formation of a loose and easily flaked corrosion product layer under continuous erosion by Cl^- and SO_2 media at high temperatures, which can seriously impair their service life (Ref 3, 4).

Multi-alloying is an important way to improve the heat resistance of TiAl. The addition of Nb, Si and other elements to TiAl alloys can significantly improve the hot corrosion resistance of the alloys by promoting an Al-rich oxide layer, but the addition of Nb and Si is not adequate to form a single Al_2O_3 barrier layer on the surface of the alloy (Ref 5). Godlewska et al. prepared TiAl alloys containing Ta at 700 °C, with excellent oxidation resistance, but significantly decreased hot corrosion resistance when the temperature was increased to 800 °C (Ref 6). Zhang et al. studied the hot corrosion resistance of Cr-containing TiAl alloy and found that the $Ti(Cr, Al)_2$ phase with low oxygen permeability formed protective Al_2O_3 in the alloy, which improved hot corrosion resistance of the TiAl alloy; however, the $Ti(Cr, Al)_2$ phase itself is less ductile and easily to cracks during the hot corrosion, which leads to more serious corrosion phenomena (Ref 7). The influences of some other alloying elements such as Mn, V and Ag on the hot corrosion behavior of TiAl alloys have also been investigated, and meaningful founds were reported; however, adding excessive alloying elements will lead to more or less negative effects such as causing deterioration to high temperature strength or room temperature ductility to TiAl alloys (Ref 8, 9).

Preparing surface protective coatings is another way to improve the hot corrosion resistance without changing the overall properties of TiAl alloys, which effectively resolves the challenges associated with TiAl alloy treatment under high temperature and the hot resistance of the coatings largely determines their service temperature and lifetime. Currently, coatings of aluminide (Ref 10-12), TiAlCr (Ref 13), MCrAlY (Ref 14), enamel (Ref 15, 16), and some noble metal-doped composites (Ref 17) have been widely used in the hot corrosion protection of TiAl alloys. Although the TiAlCr coating exhibits excellent resistance to hot corrosion, the poor bonding between the corrosive product film and the coating leads to serious corrosion in the upper part of the coating, which in turn leads to the degradation of the protective coating (Ref 18). The composition of the MCrAlY coating is flexible, and the presence of rare earth element Y in the coating can selectively form Al_2O_3 and Cr_2O_3 mixed scale with good hot corrosion resistance at high temperatures. However, the presence of Cr_2O_3 in the scale will reduce the melting point and generates Cl_2 in the presence of Cl^-, resulting in rapid dissolution and peeling off of the oxidation film and loss of protective properties (Ref 19). Although the corrosion resistance of enamel coatings is excellent, the high brittleness and mismatch with the thermal expansion coefficient of the base alloy also hinder their practical application (Ref 15).

Aluminide coatings are of great interest due to their ability to form protective Al_2O_3 films. However, drawbacks also exist in the Al_2O_3 formation coatings for hot corrosion performance. In the presence of sulfates, the continuous erosion leads to

Zekun Wei, Xuan Li, and **Wei Lv**, College of Mechanical Engineering, Sichuan University of Science and Engineering, Zigong 643000, China; and The Key Laboratory of Mechanical Structure Optimization and Material Application Technology of Luzhou, Luzhou 646300, China; **Bai Ming** and **Sheng Lai**, College of Mechanical Engineering, Sichuan University of Science and Engineering, Zigong 643000, China; **Yongquan Li**, College of Electrical and Mechanical Engineering, North Minzu University, Yinchuan 750021, China; **Xing Liu**, The Key Laboratory of Mechanical Structure Optimization and Material Application Technology of Luzhou, Luzhou 646300, China; and **Fuhua Liu**, School of Automobile and Rail Transit, Yibin Vocational and Technical College, Yibin 644003, China. Contact e-mail: biluaner@163.com.

repeated dissolution, re-deposition and re-dissolution, which rapidly consumes Al in the coating and generates a large number of holes and seriously weakens the protective performance, while in the presence of hydrochloride, Al_2O_3 reacts with Cl^- to generate volatile chloride salts and Cl_2, leading to poor adhesion and susceptibility to cracking and flaking (Ref 11, 18). Addition of Co and trace rare earth element Y to aluminide coatings can significantly improve their high-temperature oxidation resistance and hot corrosion properties (Ref 20). Elemental Co can effectively suppress the hot corrosion process by improving the adhesion and density of oxide films (Ref 21). However, elemental Y can improve the ductility of the coating and thus reduce the occurrence of cracks, while promoting the formation of protective Al_2O_3 with improved the hot corrosion resistance (Ref 22, 23). Li et al. studied the hot corrosion performance of Y-modified aluminide coatings in $(Na, K)_2SO_4$ mixed salts and showed that the Al_2O_3 film generated by the Y-modified aluminide coatings effectively blocked the internal diffusion of O and S during hot corrosion, thus significantly improving the hot corrosion performance (Ref 24). Qiao et al. prepared Co-modified aluminide coatings and found that Co enhanced the hot corrosion performance by promoting the growth of Al_2O_3 and inhibiting the diffusion of S within the coatings (Ref 25). In the present study, Al-Co-Y co-deposited coating on TiAl alloy via a pack cementation, for synergistic modification of Co-Y to generate a protective coating on the surface of TiAl alloy to facilitate the application of this alloy in high temperature structures.

2. Experimental

2.1 Materials

A TiAl alloy matrix (Ti-45Al-8Nb-0.1Y (at.%)) was prepared using a non-self-consuming method of vacuum arc melting. The surface SEM image and XRD pattern of the alloy are shown in Fig. 1. The alloy ingots were cut into 5 mm × 5 mm × 3 mm specimens by electrical discharge machining (EDM). The surface of each of the specimens was sanded smooth step-by-step using 400 #—1000 # SiC sandpaper. It was then ultrasonically cleaned in alcohol for 10 minutes and blown dry with cold air.

2.2 Preparation of the Coating

A GF17Q-I high-temperature furnace was used to prepare the coating. The powder composition was 20Al-10Co-2Y-5NaF-63Al_2O_3 (wt.%), where Al, Co and Y are the permeate elements, NaF is the activator, and Al_2O_3 is the filler. Powders were accurately weighed in proportion and then ground in a planetary ball mill for 4 h to obtain a uniform and sufficiently fine powder mixture. The coating preparation entailed burying the specimen in an alumina crucible with the powder, followed by sealing the crucible with Al_2O_3 and silica sol. The crucible containing the mixture was heated in a high-temperature furnace to 680 °C at a heating rate of 10 °C/min and held for 10 h. Then, the furnace was cooled to room temperature and removed for ultrasonic cleaning.

2.3 Hot Corrosion Tests

Hot corrosion test was conducted in an SX2-2.5-12A type muffle furnace at a temperature of 850 °C using 25% NaCl + 75% K_2SO_4 (wt.%) as the corrosion medium. During hot corrosion, the TiAl alloy and co-deposited coating specimens were placed in a corundum crucible after heating without changing the mass. In order to obtain the possible spalling corrosion products, the specimens were removed at regular intervals. The corrosion medium was promptly replenished by adding drops of the corrosion solution every 12 h to the specimen surface. At the end of the holding time, the sample was removed and cooled to room temperature. The specimen after hot corrosion was placed in distilled water for 10 min before weighing, during which it was slightly stirred to dissolve the surface salt and then dried before weighing.

2.4 Analysis and Characterization Methods

An electronic balance with an accuracy of 0.1 mg was used to measure the mass change of the specimens before and after hot corrosion, and the average value was determined by weighing the sample five times. XRD was used to determine the phase composition of the coating and corrosion product film, and SEM (JSM-6360LV) and EDS were used to analyze

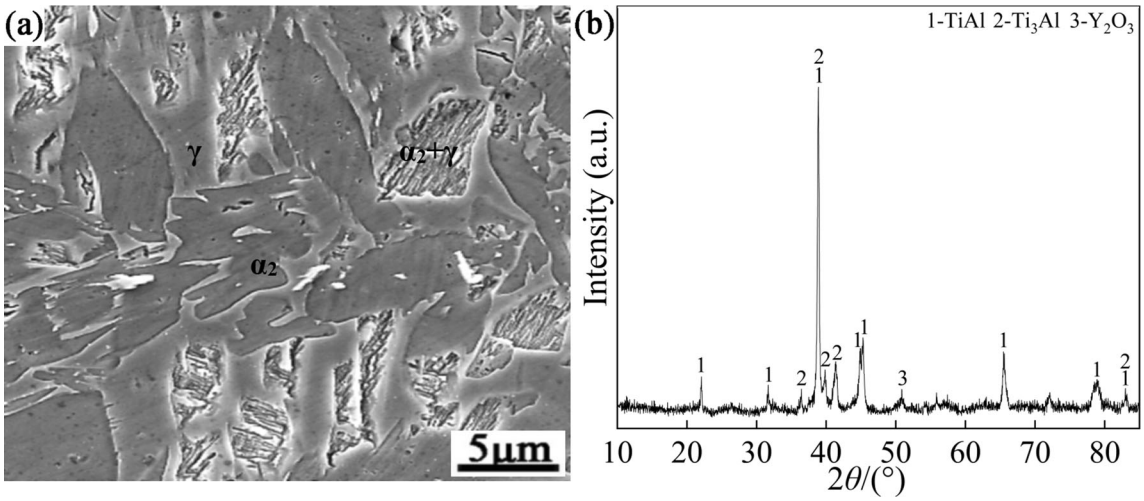

Fig. 1 Surface SEM morphology and XRD pattern of TiAl alloy

the micromorphology and chemical composition of the specimens before and after hot corrosion.

3. Results

3.1 Coating Structure

As shown in Fig. 2(a), the co-deposited coating is dense and tightly bonded to the substrate with an overall thickness about 20 μm, with the outer layer measuring about 5 μm, the middle layer approximately 11 μm and the inter-diffusion zone nearly 4 μm. The EDS composition presented in Fig. 2(b) shows that the outer layer of the coating contains 17.13Ti-73.20Al-0.19Co-0.01Y-9.47Nb (at.%). Combined with the XRD pattern shown in Fig. 2(c) and the Ti-Al-Nb ternary phase diagram (Ref 26), it is clear that the outer layer of the coating includes mainly $TiAl_3$ phase. The Ti-Al atomic content of the inner layer constitutes 32.38-63.41 at.%, and the XRD pattern of the inner layer depicted in Fig. 2(d) reveals that $TiAl_2$ forms the inner layer. The atomic ratios of Ti and Al in the inter-diffusion zone were 1:1, which when combined with the Ti-Al-Nb ternary phase diagram (Ref 26) shows that the inter-diffusion zone is composed of Al-rich γ-TiAl primarily. In addition, obvious light-colored tissues were visible in both the inner layer and the inter-diffusion zone. The analysis of EDS composition reveals higher content of Nb in these tissues than in the dark phase.

3.2 Hot Corrosion Properties

3.2.1 Hot Corrosion Kinetics. Figure 3 presents the hot corrosion kinetics of the TiAl alloy and the Al-Co-Y coating in a molten salt mixture containing 25% NaCl and 75% K_2SO_4 at 850 °C. After 1 h of hot corrosion, the mass of the substrate and Al-Co-Y coating increased by 12.5 and 4.53 mg/cm^2, respectively. With the hot corrosion proceeds, the mass gain of the substrate reached 45.32 mg/cm^2 at 15 h, while that of the Al-Co-Y coating was only 12.85 mg/cm^2. Accordingly, the corrosion products on the substrate surface were less protective compared to those formed on the coating. After hot corrosion for more than 15 h, the mass gain rate of the Al-Co-Y co-deposited coating increased rapidly. After 25 h of hot corrosion, the mass gain of the coating reached to 30.66 mg/cm^2. Obviously, the anti-hot corrosion performance of the coating weakened when hot corrosion time is over 15 h, and the specific reasons will be explained in Sect. 4.2.

3.2.2 Hot Corrosion of TiAl Alloy. Figure 4 shows the cross-sectional morphology and EDS analysis mappings of the TiAl alloy after corrosion in 25% NaCl + 75% K_2SO_4 molten

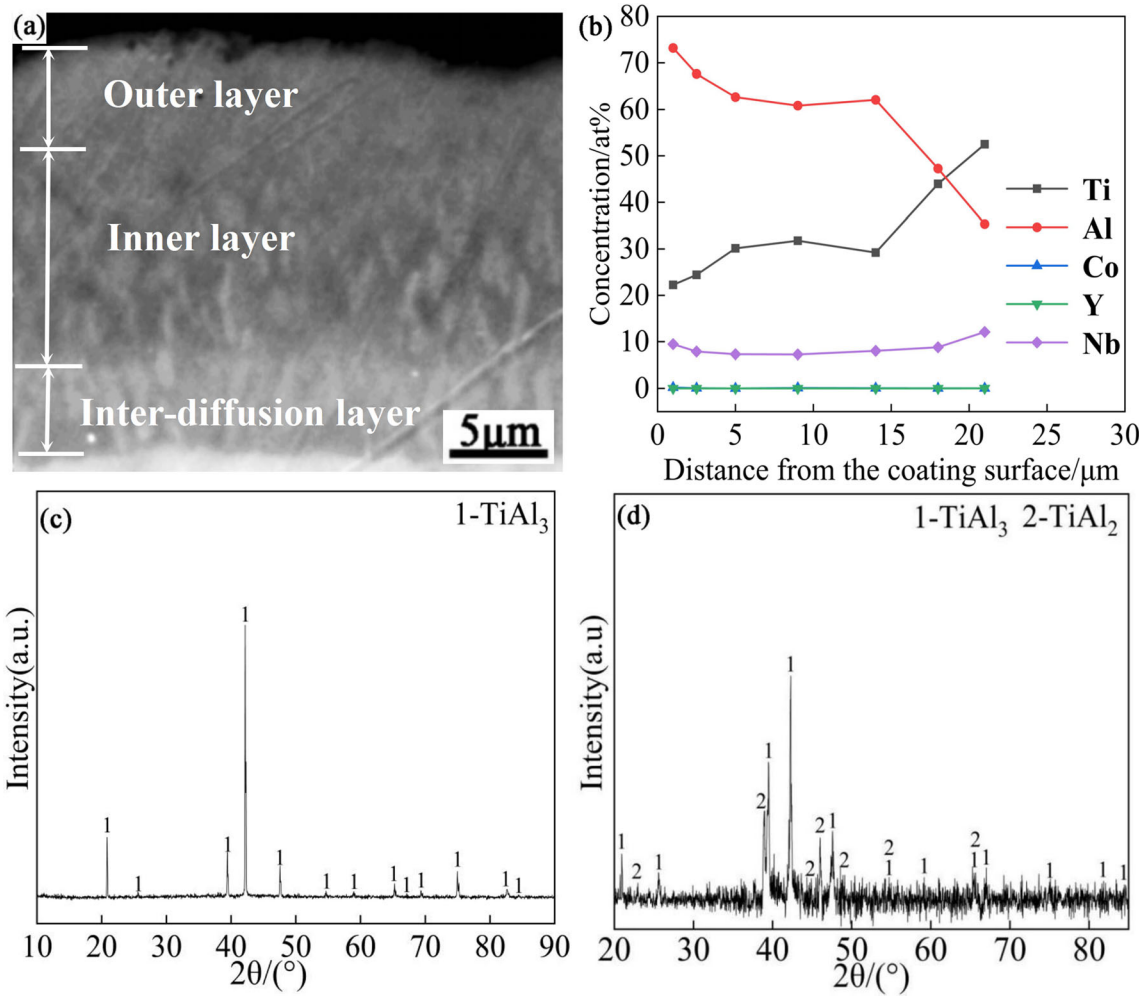

Fig. 2 Cross-sectional BSE image, elemental concentration profiles, surface and inner layer XRD pattern of Al-Co-Y co-deposited coating prepared at 680 °C for 10 h

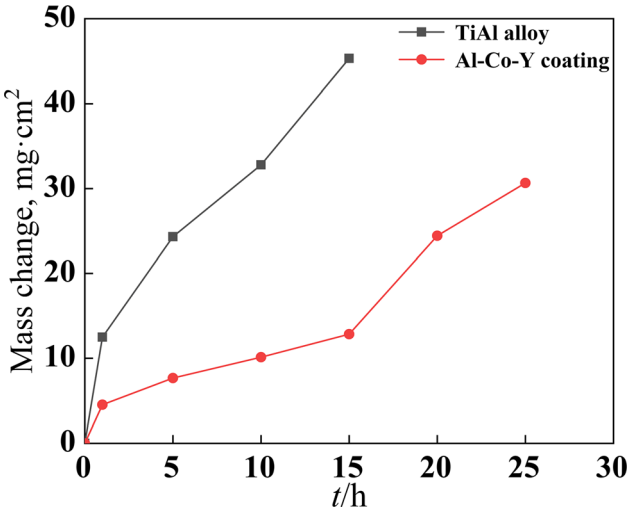

Fig. 3 Hot corrosion kinetic curves of TiAl alloy and Al-Co-Y co-deposited coating in NaCl + K_2SO_4 molten salt at 850 °C

salt at 850 °C for different times. As shown in Fig. 4(a), after 1 h of hot corrosion, a large number of corrosion gullies were formed. EDS analysis revealed that the typical composition of corrosion products in the upper layer of the alloy was 20.39Ti-9.83Al-21.25Nb- 0.65Y-42.26O-0.68Na-0.69K-4.26Cl (at.%). When combined with the XRD results shown in Fig. 5, it can be seen that the corrosion product was mainly TiO_2. The EDS analysis mapping of Fig. 4(a_1) shows an obvious enrichment of Nb element in the corrosion area along the corrosion gullies. EDS did not reveal the presence of S in this region, whereas the content of Y in the corrosion region was significantly higher than that of the substrate, presumably due to inhibition of diffusion of S by Y during the early stage of corrosion, thus slowing down the corrosion rate.

Figure 4(b) shows that the thickness of the corrosion product film reached about 20 μm after 5 h of hot corrosion, with obvious cracking and loosening of the corrosion product film. EDS analysis shows that the corrosion products were mainly TiO_2 and Al_2O_3. After 5 h of hot corrosion, the corrosion gully extended deeper into the substrate, suggesting an obvious preferential corrosion. As shown in Fig. 6(a), the corrosion gully extending deep into the substrate shows a lamellar organization similar to that of the TiAl alloy, indicating that the alloy was preferentially corroded in the presence of molten mixture of NaCl and K_2SO_4. Zhao et al. also showed that TiAl alloys showed significant preferential corrosion, where the α_2 phase was preferentially corroded and the corrosion products generated significant corrosion pits in the substrate along the preferential corrosion path (Ref 27). The result of EDS also revealed white Nb-rich bands enclosing the preferentially corroded areas. After 10 h of corrosion, the corrosion products on the surface of the alloy were loosened and cracked extensively, as shown in Fig. 4(c). Hot corrosion for 15 h resulted in serious cracking of the corrosion product and the substrate. As shown by the EDS mapping in Fig. 4(d_1), the substrate underwent severe internal sulfation and oxidation, with the corrosion product film showing an overall multilayered structure. EDS analysis revealed the following corrosion product layers from top to bottom: TiO_2, Al_2O_3, TiO_2 and TiO_2 + Al_2O_3.

3.2.3 Hot Corrosion of Al-Co-Y Co-deposited Coating. Figure 7 shows the cross-sectional morphology, EDS analysis mappings and surface morphology of the Al-Co-Y coating after 1 h, 5 h, 15 h and 25 h of hot corrosion in 25% NaCl + 75% K_2SO_4 molten salt at 850 °C. As shown in Fig. 7(a), after 1 h of hot corrosion of the coating, a continuous and dense corrosion product with a thickness of about 2 μm was formed. EDS analysis determined that the typical dark phase has a composition of 9.91Ti-34.07Al-1.98Nb-0.08Co-0.08Y-46.66O-0.81Na-0.41K-0.36Cl (at.%). When combined with the XRD pattern shown in Fig. 8, it can be seen that the dark phase was Al_2O_3. The surface scan revealed an enriched band of S above the Al_2O_3 film, indicating that Al_2O_3 effectively blocked the internal diffusion of S below the corrosion product film. A grayish-white Ti enrichment band was formed, presumably due to the generation of alumina at the beginning of the hot corrosion, resulting in an increase in the proportion of Ti in the coating. The Al_2O_3 layer can effectively blocked the outward diffusion of Ti, thus enriching Ti. After 1 h of hot corrosion, the surface of the coating was mainly consisted of Al_2O_3, as shown in Fig. 7(b).

As the hot corrosion continued, the protective Al_2O_3 film gradually thickened to about 4 μm after 15 h of hot corrosion. However, a bright white Co-enriched phase appeared in the corrosion product film, which was uniform and dense and always maintained good bonding with the coating. However, a few continuous dark phases appeared in the coating below the corrosion product film. Based on EDS, the typical composition of the dark phases was 7.35Ti-26.82Al-0.56Nb-0.76Co-64.40O-0.09Na-0.01K (at.%), indicating local internal oxidation in the coating. As shown in Fig. 7(d) and (f), the surface of corrosion products mainly consisted of scale-like Al_2O_3. However, increasing the hot corrosion time from 5 to 15 h led to an obvious elevation in the scale-like Al_2O_3 on the surface. Further, after 15 h of corrosion, the scale-like alumina showed a few fine pores, which provided channels for the diffusion of O and S during the hot corrosion, resulting in adverse effects. These findings were confirmed by the internal oxidation in the coating.

Figure 7(g) and (h) shows the cross-sectional and surface morphology of the Al-Co-Y coating after 25 h of hot corrosion. As shown in Fig. 7(g), the cross-sectional morphology of the coating specimen after 25 h of hot corrosion was changed dramatically to a multilayered structure, the thickness is about 150 μm, and an overall looseness and a large number of cracks. The cracked corrosion products and substrate have no protective ability due to serious internal oxidation and sulfide formation. After 25 h of hot corrosion, the outermost layer of the corrosion product film appeared bright gray, interspersed with a few black particles. EDS analysis showed that the typical composition of the bright gray outer layer was 8.95Ti-6.94Al-11.41Nb-0.12Y-57.60O-11.85Na-0.28K-2.56S-0.29Cl (at.%). Combined with the XRD patterns presented in Fig. 8, the outer layer of the corrosion film was mainly composed of $NaNbO_3$ and a small amount of TiO_2. In order, the outer layer to the bottom is the TiO_2 layer, Al_2O_3 layer and Al_2O_3 + TiO_2 layer. Some black phases appeared in the outer layer, as shown in Fig. 9(a), and the results of EDS analysis are presented in Table 1 (Point 1), which showed that the Na content of the black phase reached 23.96 (at.%). The morphology presented in Fig. 7(h) reveals pitting corrosion and holes on the corrosion

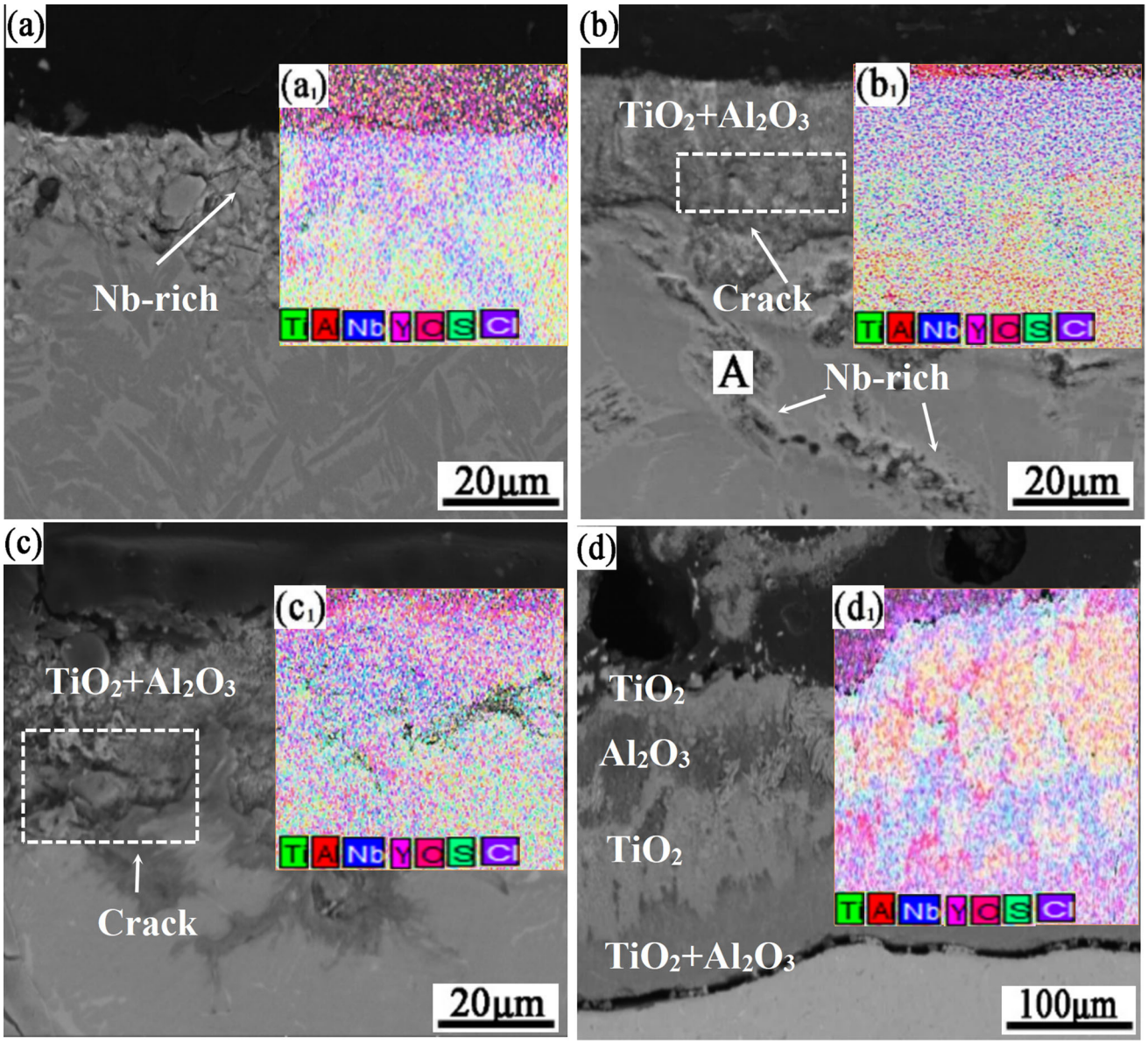

Fig. 4 Cross-sectional BSE images and EDS analysis mappings of TiAl alloys after hot corrosion for (a) 1 h, (b) 5 h, (c) 10 h and (d) 15 h

product surface after 25 h of hot corrosion. A bright white Y-enriched slender region (Fig. 9(b)) can be found at the junction of the TiO_2 and Al_2O_3 layers of the corrosion product film, as the Y content in this area was as high as 4.12 at.% (point 2 in Table 1). In the corrosion regions C (Fig. 9(c)) and D (Fig. 9(d)) close to the substrate, an obvious phenomenon of preferential corrosion was observed. The corrosion region at C showed a lamellar structure, and a large amount of light-colored phase and a small amount of dark phase distributed in the two lamellar structures. Based on the EDS analysis presented in Table 1 (Point 3 and 4), the light phase was TiO_2, while the dark phase was Al_2O_3, because the Ti content in the α_2 phase is as high as 75 at.%, which preferentially corroded under the action of O, S and other corrosive media, generating TiO_2 with poor adhesion and protection. In addition, based on distribution of Nb (Fig. 9(d_1)) and S (Fig. 9(d_2)) in the D region that Nb and S elements were distributed along the formed corrosion pits and penetrated deeply into the substrate. The sulfides generated accelerated the oxidation of the substrate, as sulfides are easier to oxidize than monolithic metals, forming loose and discontinuous oxidation products (Ref 28), which resulted in cracking. Figure 10 shows the BSE image of the coating specimen at E (Fig. 10(b)), suggesting that the protective Al_2O_3 film formed during the corrosion incubation period underwent drastic dissolution and rupture. Combined with the BSE image at E, the findings reveal a teardrop-shaped TiO_2 region formed in the ruptured alumina film, which was connected to the TiO_2 layer above and below the alumina layer, indicating that dissolution of the protective alumina layer contributed to serious corrosion of the alloy.

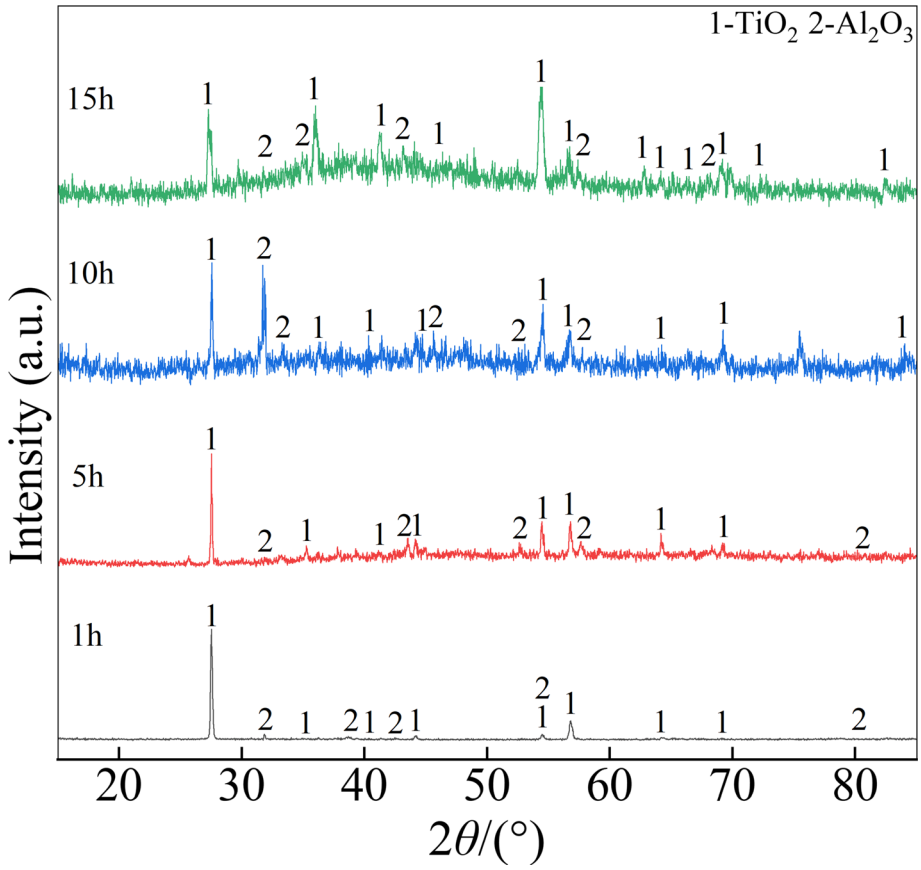

Fig. 5 Surface XRD patterns of TiAl alloy after hot corrosion

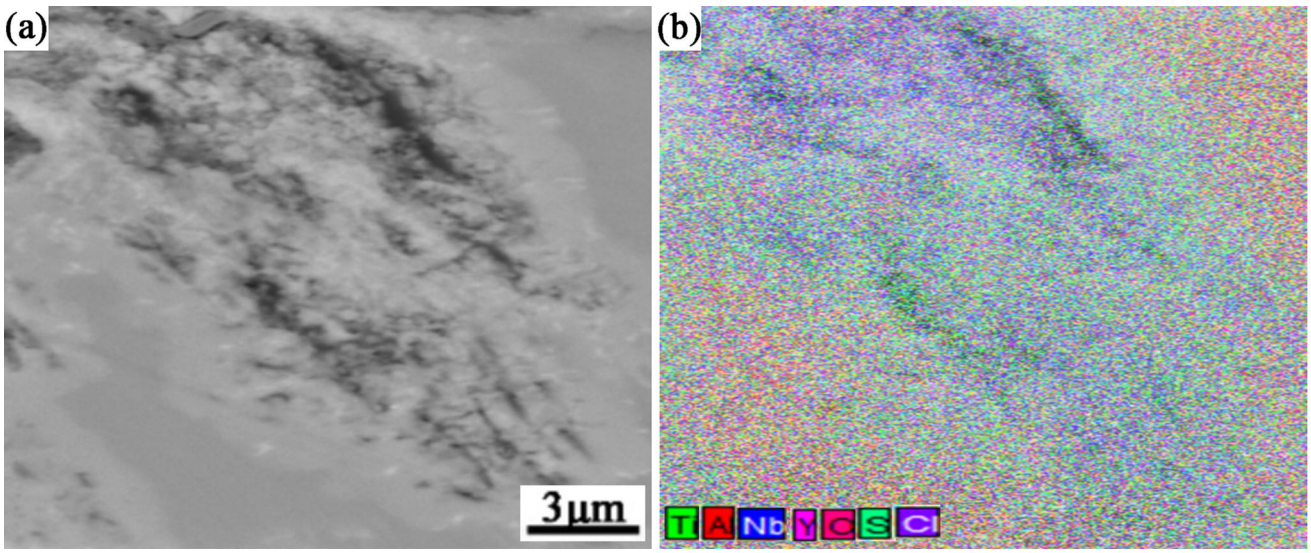

Fig. 6 Enlarged BSE morphology and EDS analysis mapping at section A in Fig. 4(b)

4. Discussion

4.1 Hot Corrosion Mechanisms of the TiAl Alloy

Hot corrosion represents accelerated oxidation in the presence of sulfate and NaCl or one of the salts (Ref 29, 30). The hot corrosion process can be divided into an incubation phase and an extension phase. In the incubation phase, a continuous and dense protective corrosion product film is formed and maintained on the surface of the alloy. The rupture of the film and the acid–base melting represent the end of the incubation phase and the beginning of the extension phase, and the type and nature of the product film formed by hot corrosion determine its resistance to corrosion (Ref 31). The O and S elements play the most important roles in the whole corrosion process (Ref 14). TiAl alloys exhibit strong hot corrosion

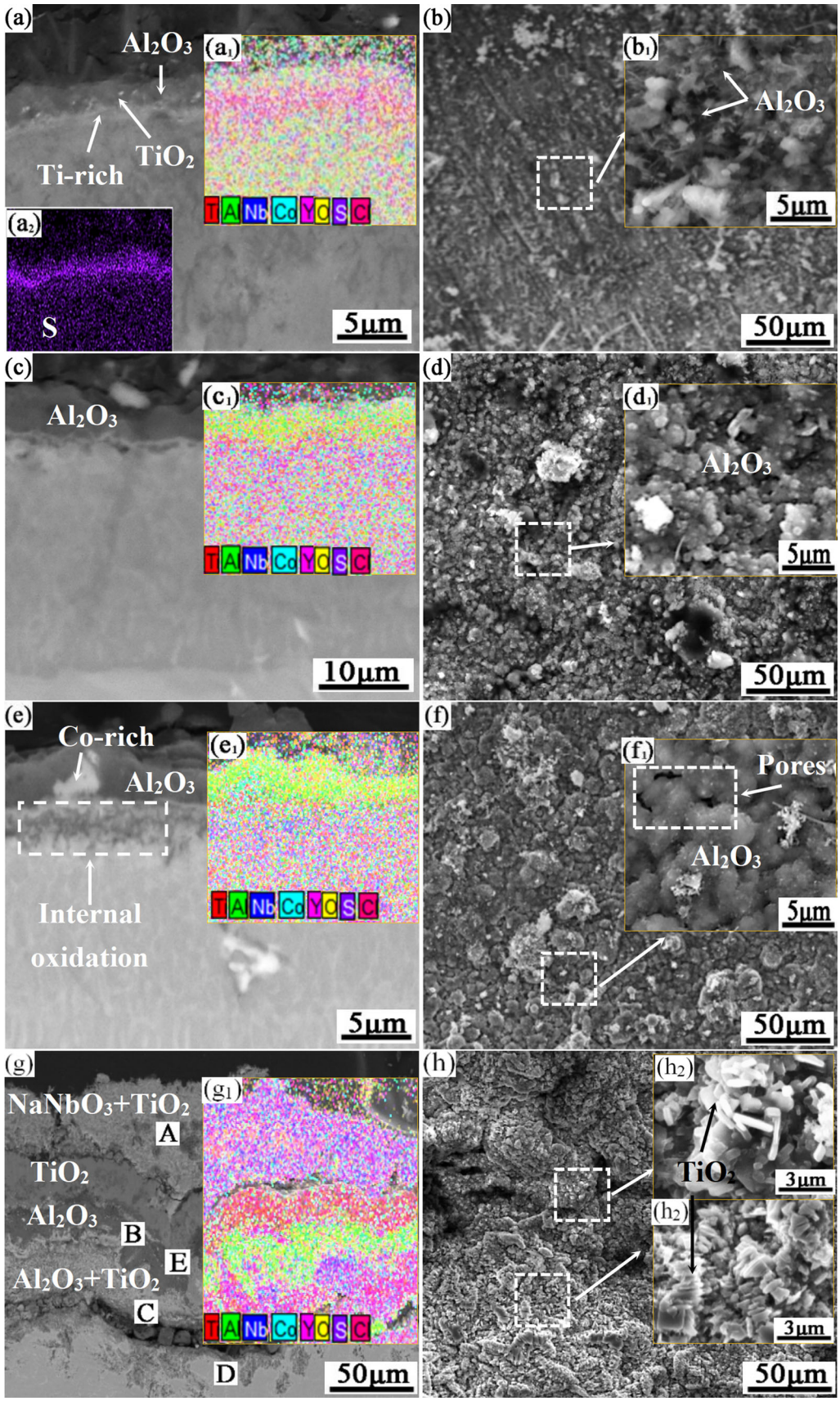

Fig. 7 Cross-sectional BSE images, EDS analysis mappings, and surface morphology of Al-Co-Y co-deposited coatings after hot corrosion for (a) (b) 1 h, (c) (d) 5 h, (e) (f) 15 h, (g) (h) 25 h

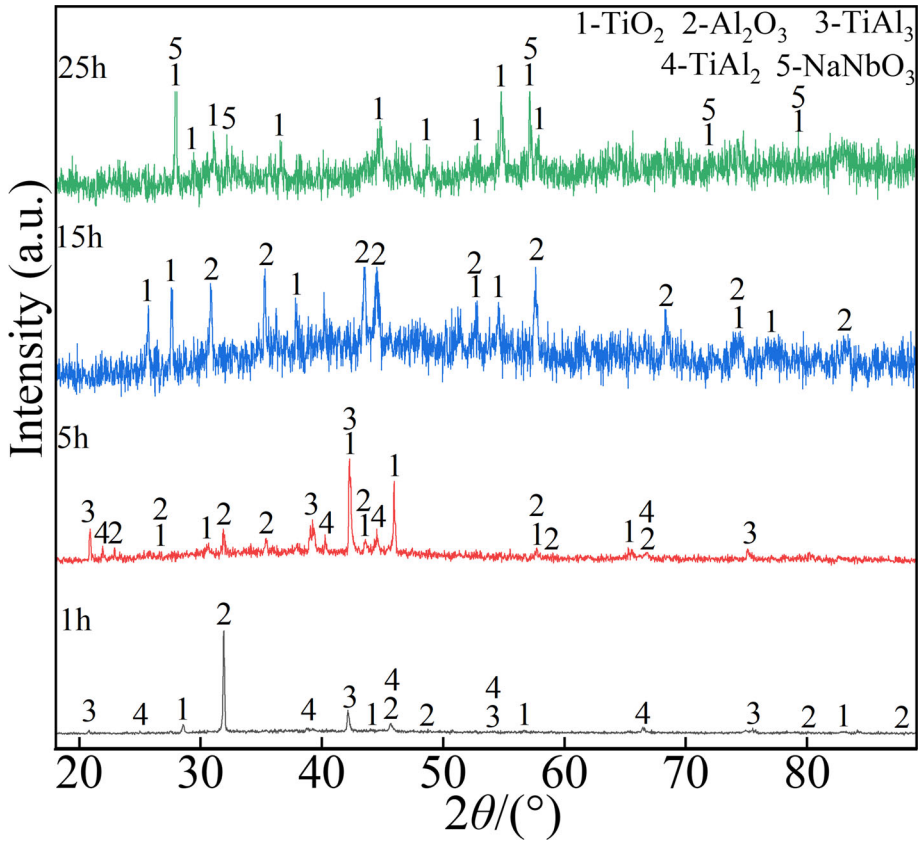

Fig. 8 Surface XRD patterns of the Al-Co-Y co-deposited coatings after hot corrosion for different times

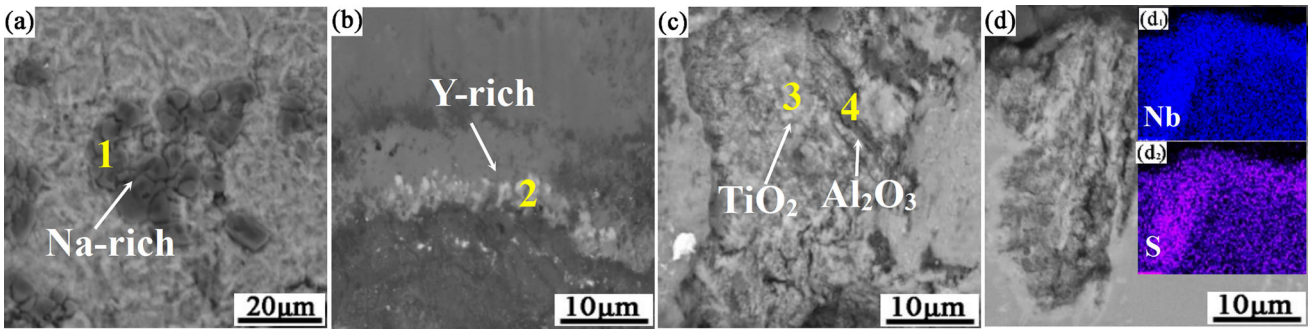

Fig. 9 Enlarged BSE images of the Al-Co-Y co-deposited coating at sections A to D in Fig. 7(g). (a) Section A, (b) section B, (c) section C, (d) section D

Table 1 Compositions of the points 1-4 in Fig. 9 determined by EDS analysis

	Composition, at.%									
Area	**Ti**	**Al**	**Nb**	**Co**	**Y**	**O**	**Na**	**K**	**S**	**Cl**
1	2.58	0.89	2.99	…	0.06	60.14	23.96	0.04	9.30	0.04
2	18.34	6.78	3.73	0.02	4.12	66.59	0.34	0.05	…	0.05
3	21.87	9.95	15.73	0.04	0.15	50.16	0.73	0.23	0.96	0.18
4	5.19	21.05	2.76	…	…	70.84	0.10	0.04	0.01	0.01

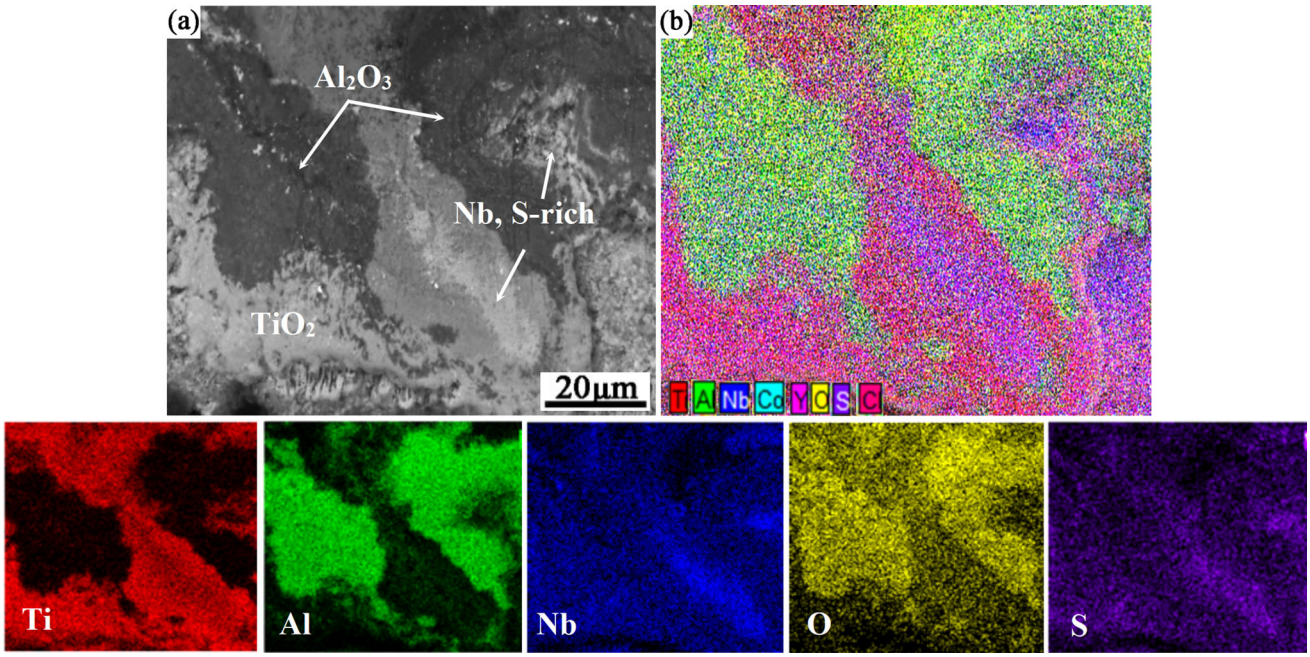

Fig. 10 Enlarged BSE morphology and EDS analysis mappings at section E in Fig. 7(g)

resistance in sulfates, whereas in mixed salts, severe corrosion occurs due to the inability to form protective Al_2O_3 films (Ref 32).The reactions that occur in the hot corrosion process of TiAl alloy in mixed molten salts of 25% NaCl + 75% K_2SO_4 are as follows:

$$2K_2SO_4 \rightarrow 2K_2O + 2SO_2 + O_2 \quad \text{(Eq 1)}$$

From the above equation, it is clear that the molten salt is a high S and low O system during corrosion. In the early stages of hot corrosion, preferential corrosion occurs in the alloy with a lamellar α_2 phase, a highly reactive Ti-rich phase that reacts with the inwardly diffusing O_2 (Ref 27):

$$Ti + O_2 \rightarrow TiO_2 \quad \text{(Eq 2)}$$

$$4Al + 2O_2 \rightarrow 2Al_2O_3 \quad \text{(Eq 3)}$$

Due to the presence of NaCl in the corrosive medium, metal oxides, metal chlorides and metal sulfides are formed simultaneously, and sodium chloride reacts with Ti and Al as follows (Ref 7, 33):

$$4NaCl + 2Al_2O_3 + O_2 \rightarrow 4NaAlO_2 + 2Cl_2 \quad \text{(Eq 4)}$$

$$2NaCl + 2TiO_2 + 2O_2 \rightarrow 2NaTiO_4 + Cl_2 \quad \text{(Eq 5)}$$

As the Cl_2 generated by the reaction diffuses and is transported, chlorides are formed (Ref 7):

$$Ti + 2Cl_2 \rightarrow 4TiCl_4 \quad \text{(Eq 6)}$$

$$2Al + 3Cl_2 \rightarrow 2AlCl_3 \quad \text{(Eq 7)}$$

The generated chlorides volatilize at hot corrosion temperatures due to their low boiling points (135.9 °C for $TiCl_4$ and 178 °C for $AlCl_3$). They are thermodynamically unstable and may further react with O_2 to generate the corresponding oxides to generate Cl_2, which is harmful to the substrate:

$$TiCl_4 + O_2 \rightarrow TiO_2 + 2Cl_2 \quad \text{(Eq 8)}$$

$$4AlCl_3 + 3O_2 \rightarrow 2Al_2O_3 + 6Cl_2 \quad \text{(Eq 9)}$$

A portion of the generated Cl_2 will continue to participate in the reactions (6) and (7), forming a self-circulating system and accelerating the corrosion of the alloy. However, the presence of gasses such as Cl_2, SO_2 and O_2 in the reaction system loosens the corrosion film and facilitates the diffusion of elements such as S and O. In the substrate, although the activity of Ti is lower than that of Al, the diffusion rate of Ti is substantially higher than that of Al. In the case of hot corrosion, the rapidly diffusing Ti combines with O_2 diffusing within the phase to generate TiO_2. The serious internal oxidation leads to drastic and catastrophic substrate corrosion and a rapid increase in corrosion weight gain and results in a corrosion product film with mixed TiO_2 and Al_2O_3 and a multilayered structure.

4.2 Hot Corrosion Mechanisms of the Al-Co-Y Co-deposited Coating

The coating specimen reacts to form a film of corrosion products dominated by Al_2O_3 at the beginning of hot corrosion due to the high Al content on the surface (Fig. 7(a)):

$$4TiAl_3 + 3O_2 \rightarrow 4TiAl_2 + 2Al_2O_3 \quad \text{(Eq 10)}$$

Due to the presence of sulfate, Al_2O_3 reacts with the O^{2-} produced by the decomposition of sulfate, resulting in its dissolution:

$$Al_2O_3 + O^{2-} \rightarrow 2AlO_2^- \quad \text{(Eq 11)}$$

Then, AlO^{2-} diffuses from the molten salt/coating deposition interface to the corrosion product/air interface, where the alkalinity of the molten salt is low and Al_2O_3 is redeposited via the decomposition of AlO^{2-} (Ref 25):

$$2AlO_2^- \rightarrow Al_2O_3 + O^{2-} \quad \text{(Eq 12)}$$

The dense Al_2O_3 film effectively prevents the diffusion of O^{2-}, thus increasing the alkalinity of the corrosion product/air interface, which in turn promotes the reaction (11), ensuring dynamic equilibrium between dissolution and deposition of Al_2O_3 (Ref 25, 34). However, due to the presence of NaCl in the molten salt, reaction (4) also proceeds simultaneously, causing the dissolution of Al_2O_3. Studies have shown that NaCl in the molten salt is the main factor contributing to the failure of the protective corrosion product film dissolution (Ref 19, 35). Due to the above reactions, the growth of Al_2O_3 is slowed. As shown in Fig. 7(c), the thickness of the alumina film was only 3 μm after 5 h of hot corrosion.

By the middle and late stages of the corrosion incubation period, in order to maintain the generation of Al_2O_3 on the surface, a large number of Al atoms diffuse outward, and the outermost layer of $TiAl_3$ in the coating layer continues to degrade into $TiAl_2$. The continuous erosion of the corrosion medium leads to the appearance of fine pores on the surface of the corrosion film, which facilitates diffusion of O, S and other corrosion media, resulting in local internal oxidation, as shown in Fig. 7(e).

During the late stage of the corrosion incubation, due to the continuous dissolution of NaCl on the corrosion product, the Al_2O_3 layer is disrupted and the hot corrosion is extended. As shown in Fig. 10, the ruptured Al_2O_3 film releases a large amount of O, S and other corrosion media into the substrate, and the outward diffusion of Ti generates a loose and poorly adherent TiO_2, thus forming a multilayered film. The outermost layer of the corrosion product film has been confirmed as $NaNbO_3$ and TiO_2 mixtures, caused by the following reaction in a low oxygen partial pressure and sodium-rich system (Ref 3):

$$Nb_2O_5 + 2Na^+ + O^{2-} \rightarrow 2NaNbO_3 \quad \text{(Eq 13)}$$

Both Co and Y promote the selective oxidation of Al, resulting in the formation of a continuous Al_2O_3 protective layer (Ref 36-40). The hot corrosion experiments of the substrate did not show the formation of continuous Al_2O_3 despite the presence of Y in the substrate, which should be a result of the rapid dissolution of Al_2O_3 in the presence of sulfate and chloride salts. In contrast, in the coated specimens, due to the high Al content in the coating and the synergistic effect of Co-Y, a continuous dense Al_2O_3 layer was formed, which effectively improved the anti-hot corrosion performance of the TiAl alloy. As shown by the EDS analysis mapping at each hot corrosion stage, the distribution of Co and Y in the coating was uniform. Zhou et al. reported that the addition of Y promoted the diffusion of Co in the coating, which resulted in a uniform distribution of Co (Ref 40). The EDS analysis mapping revealed no obvious internal sulfidation during the corrosion incubation, even during prolonged corrosion. The internal sulfidation occurred only in the preferential corrosion region of the alloy, because the Al_2O_3 layer blocked the S diffusion, while Co retarded the S diffusion and slowed down the rate of sulfidation–oxidation, which in turn enhanced the hot corrosion resistance of the coating (Ref 25).

5. Conclusions

The Al-Co-Y co-deposited coating with a multilayered structure comprising $TiAl_3$, $TiAl_2$ and an inter-diffusion γ-TiAl layer was prepared on TiAl alloy by pack cementation process. During hot corrosion in 25% NaCl + 75% K_2SO_4 molten salt at 850 °C, preferential corrosion of both the TiAl alloy and Al-Co-Y co-deposited coating specimens occurred. For the TiAl alloy, the α_2 phase, due to its high Ti content, first reacted with O, S and other corrosive media to generate corrosion products with poor density and adhesion, resulting in severe corrosion. For the Al-Co-Y co-deposited coating, a dense Al_2O_3 film formed during the incubation period, which inhibited the internal diffusion of O and S elements and the external diffusion of Ti and effectively improved the anti-hot corrosion performance of the alloy. However, with prolonging the hot corrosion process, the Al_2O_3 film was gradually dissolved and ruptured under the action of mixed salts, losing its protective properties.

Acknowledgments

This work was supported by the National Natural Science Foundation of China (No. 51961003), the Major Project of Science and Technology Department of Sichuan province (No. 2022YFSY0036), the Major Project of Science and Technology Department of Shaanxi Province (No. 2020GY-324), the Project of Science and Technology Department of Yibin (No. 2021GY-006), the Project of Yibin Vocational and Technical College (YB-ZYSC18-12, ZRKY21ZD-09), and the Project of the Key Laboratory of Mechanical Structure Optimization & Material Application Technology of Luzhou (SCHYZSA-2022-01, SB-2022-01, SCHYZSB-2022-02)

References

1. M. Yamaguchi, H. Inui and K. Ito, High-Temperature Structural Intermetallics, *Acta Mater.*, 2000, **48**, p 307–322.
2. M. Yoshihara and Y.W. Kim, Oxidation Behavior of Gamma Alloys Designed for High Temperature Applications, *Intermetallics*, 2005, **13**, p 952–958.
3. Y.J. Xi, Y.J. Liu, Z.X. Wang and J.B. Lu, Effects of TiAl Coating on Hot Corrosion and Electrochemical Corrosion of Ti_3Al Alloy, *J. Mater. Eng.*, 2009, **30**, p 49–52.
4. X.Q. Long, Mechanism of Hot Corrosion in High Temperature Parts of Aeroengine, *Total Corros. Control*, 2003, **17**, p 9–14.
5. C.L. Zeng, J.Q. Zhang, W.T. Wu, J.S. Wu, G.H. Qiu and D. Li, Effect of Alloying Elements on Hot Corrosion Resistance of Ti_3Al Intermetallic Compound, *Corros. Sci. Prot. Tech.*, 1995, **7**, p 29–34.
6. E. Godlewska, M. Mitoraj and M. Leszczynska, Hot Corrosion of Ti-46Al-8Ta (at.%) Intermetallic Alloy, *Corros. Sci.*, 2014, **78**, p 63–70.
7. K. Zhang, Z.W. Li and W. Gao, Hot Corrosion Behaviour of Ti-Al Based Intermetallics, *Mater. Lett.*, 2002, **57**, p 834–843.
8. G.X. Jin, L.J. Qiao and K.W. Gao, Effect of Mn and V on Hot Corrosion of TiAl Alloy, *Acta Metall. Sin.*, 2004, **40**, p 179–184.
9. W. Gao, K. Zhang and J. Liang, Molten Salt Vapour Corrosion of Ti-Al-Ag Intermetallics, *Intermetallics*, 2004, **12**, p 539–544.
10. B.L. Rem, Q. Miu, W.P. Liang, J.J. Xia and R.Y. Hu, Effects of NaCl Salt on Hot Corrosion Behaviors of Aluminized Layer Prepared on Ti_2AlNb Alloy, *Chin. Surf. Eng.*, 2016, **29**, p 41–47.
11. B.L. Ren, W.P. Liang, Q. Miu, W. Liu, W.B. Chen, J.J. Xia and Y. Huang, Thermal Corrosion Resistance of Ti_2AlNb Alloy Surface Deposited with Al Coating, *J. Mater. Prot.*, 2016, **49**, p 1–4.
12. M.P. Bacos, M. Thomas, J.L. Raviart, A. Morel, S. Mercier and P. Josso, Influence of an Oxidation Protective Coating upon Hot

Corrosion and Mechanical Behaviour of Ti-48Al-2Cr-2Nb Alloy, *Intermetallics*, 2011, **19**, p 1120–1129.
13. Y.J. Xi, Y.J. Liu, Z.X. Wang and J.B. Lu, Effect of TiAl Coating on Hot Corrosion Protection of Ti_3Al Alloy, *Nonferrous Met. (Extractive Metallurgy)*, 2011, **6**, p 29–32.
14. Z.J. Tian, X.S. Gao, Y.H. Huang, Z.D. Liu, D.L. Shen and D.S. Wang, Study on Hot Corrosion Behavior of Plasma-Sprayed NiCoCrAl-Y_2O_3 Coating on TiAl Alloy Surface, *Rare Met. Mater. Eng.*, 2010, **39**, p 1439–1442.
15. Z.L. Tang, F.H. Wang and W.T. Wu, Effect of Al_2O_3 and Enamel Coatings on 900 °C Oxidation and Hot Corrosion Behaviors of Gamma-TiAl, *Mater. Sci. Eng. A*, 2000, **1**, p 70–75.
16. C.H. Guan, Z.L. Tang and F.H. Wang, Effect of Enamel Coating on Oxidation and Hot Corrosion Resistance of Ti-24Al-14Nb-3V, *Chin. J. Mater. Res.*, 2000, **14**, p 75–80.
17. X.X. Ma, Y.H. He, J.P. Lin, D.R. Wang and J. Zhang, Effect of a Magnetron Sputtered (Al_2O_3–Y_2O_3)/(Pt–Au) Laminated Coating on Hot Corrosion Resistance of 8Nb-TiAl Alloy, *Surf. Coat. Technol.*, 2012, **206**, p 2690–2697.
18. Z.L. Tang, F.H. Wang and W.T. Wu, Effect of a Sputtered TiAlCr Coating on Hot Corrosion Resistance of Gamma-TiAl, *Intermetallics*, 1999, **7**, p 1271–1274.
19. X.Y. Lu, D.Q. Yu, S.M. Jiang, S.C. Liu, J. Gong and C. Sun, Hot Corrosion Behavior of a (NiCoCrAlYSiB + AlSiY) Composite Coating, *Acta Metall. Sin.*, 2012, **48**, p 461–468.
20. P. Zhang and X.P. Guo, Effect of Al Content on the Structure and Oxidation Resistance of Y and Al Modified Silicide Coatings Prepared on Nb-Ti-Si Based Alloy, *Corros. Sci.*, 2013, **71**, p 10–19.
21. X.Q. Xie, X. Li, W. Lv, S. Lai, Y. Liu, J.J. Li and W.L. Xie, Effect of Co on Microstructure and High Temperature Oxidation Resistance of Ti45Al-8Nb-03Y Alloy, *J. Mater. Eng.*, 2022, **50**, p 101–108.
22. Y.Q. Li, F.Q. Xie and X.Q. Wu, Microstructure and High Temperature Oxidation Resistance of Si-Y Co-deposition Coatings Prepared on TiAl Alloy by Pack Cementation Process, *Trans. Nonferrous Met. Soc. China*, 2015, **25**, p 803–810.
23. P. Zhang and X.P. Guo, A comparative Study of Two Kinds of Y and Al Modified Silicide Coatings on an Nb-Ti-Si Based Alloy Prepared by Pack Cementation Technique, *Corros. Sci.*, 2011, **53**, p 4291–4299.
24. Y.Q. Li, J.L. Li, C. Qin, L. Jiang and G.H. Geng, Microstructure and Hot Corrosion Behavior of Al-Ce-Y Coatings on DZ125 Nickel-Based Alloy Prepared by Pack Cementation Process, *J. Cent. South Univ.*, 2020, **27**, p 381–387.
25. M. Qiao and C.G. Zhou, Hot Corrosion Behavior of Co Modified NiAl Coating on Nickel Base Superalloys, *Corros. Sci.*, 2012, **63**, p 239–245.
26. G.L. Chen, X.T. Wang, S.M. Hao and J.J. Ding, Investigation on the 1000, 1150 and 1400 °C Isothermal Section of the Ti-Al-Nb System, *Intermetallics*, 1996, **4**, p 13–22.
27. W.Y. Zhao, B.W. Xu, Y. Ma and S.K. Gong, Inter-Phase Selective Corrosion of γ-TiAl Alloy in Molten Salt Environment at High Temperature, *Prog. Nat. Sci. Mater. Int.*, 2011, **21**, p 322–329.
28. Y. Li, J.T. Guo, C. Yuan, H.C. Yang, N. Xu and Z.M. Shen, Hot Corrosion of Nickel-Base Superalloy K35 at 800 °C, *J. Chin. Soc. Corros. Prot.*, 2005, **25**, p 250–255.
29. N. Eliaz, G. Shemesh and R.M. Latanision, Hot Corrosion in Gas Turbine Components, *Eng. Fail. Anal.*, 2002, **9**, p 31–43.
30. N.S. Bornstein and M.A. Decrescente, The Role of Sodium in the Accelerated Oxidation Phenomenon Termed Sulfidation, *Metall. Trans.*, 1971, **2**, p 2875–2883.
31. D.L. Guan, H.Z. Lu, Y.T. Xiao and C.X. Shi, The Effect of Cobalt on the Hot Corrosion Behavior of Ni-Base Superalloys, *J. Chin. Soc. Corros. Protect.*, 1981, **1**, p 49–60.
32. Z.L. Tang, F.H. Wang and W.T. Wu, Hot Corrosion Behavior of TiAl Intermetallics in Molten Salts, *J. Chin. Soc. Corros. Prot.*, 1997, **17**, p 233–236.
33. G.X. Jin, J.X. Li, H.B. Qi, L.J. Qiao and K.W. Gao, Investigation of Hot Corrosion of (Al, Mn)$_3$Ti-2V Intermetallics, *Acta Metall. Sin.*, 2004, **40**, p 185–190.
34. H.Y. He, Z.J. Liu, W. Wang and C.G. Zhou, Microstructure and Hot Corrosion Behavior of Co-Si Modified Aluminide Coating on Nickel Based Superalloys, *Corros. Sci.*, 2015, **100**, p 466–473.
35. Z. Yao and M. Marck, NaCl-Induced Hot Corrosion of a Titanium Aluminide Alloy, *Mater. Sci. Eng. A*, 1995, **192**, p 994–1000.
36. Z.X. Shi, S.Z. Liu and J.R. Li, Effect of Yttrium on Gas Hot Corrosion Resistance of Single Crystal Superalloy, *Chin. Rare Earths*, 2016, **37**, p 81–85.
37. V. Babic, C. Geers and I. Panas, Reactive Element Effects in High-Temperature Alloys Disentangled, *Oxid. Met.*, 2020, **93**, p 229–245.
38. H.X. Li, M. Qiao and C.G. Zhou, Formation and Cyclic Oxidation Resistance of Hf-Co-Modified Aluminide Coatings on Nickel Base Superalloys, *Mater. Chem. Phys.*, 2014, **143**, p 915–920.
39. M. Qiao and C.G. Zhou, Codeposition of Co-Al-Y on Nickel Base Superalloys by Pack Cementation Process, *Corros. Sci.*, 2013, **75**, p 454–460.
40. X.S. Zhao and C.G. Zhou, Effect of Y_2O_3 Content in the Pack on Microstructure and Hot Corrosion Resistance of Y-Co-modified Aluminide Coating, *Corros. Sci.*, 2014, **86**, p 223–230.